Continental Shelf Research 60S (2013) S185–S197

Contents lists available at SciVerse ScienceDirect

Continental Shelf Research

journal homepage: www.elsevier.com/locate/csr

Research papers

Seasonal variations in erodibility and sediment transport potential in a mesotidal channel-flat complex, Willapa Bay, WA

Patricia L. Wiberg [a,*], Brent A. Law [b], Robert A. Wheatcroft [c], Timothy G. Milligan [b], Paul S. Hill [d]

[a] Department of Environmental Sciences, University of Virginia, PO Box 400123, Charlottesville, VA 22904-4123, United States
[b] Fisheries and Oceans Canada, Bedford Institute of Oceanography, Dartmouth, Nova Scotia, Canada B2Y 4A2
[c] College of Earth, Ocean and Atmospheric Sciences, Oregon State University, Corvallis, OR, 97331, United States
[d] Department of Oceanography, Dalhousie University, Halifax, Nova Scotia, Canada B3H 4J1

ARTICLE INFO

Article history:
Received 5 August 2011
Received in revised form
5 July 2012
Accepted 27 July 2012
Available online 4 August 2012

Keywords:
Tidal flats
Erodibility
Sediment transport
Willapa Bay
Mudflats
Estuary

ABSTRACT

Measurements of erodibility, porosity and sediment size were made three times over the course of a year at sites within a muddy, mesotidal flat-channel complex in southern Willapa Bay, WA, to examine spatial and seasonal variations in sediment properties and transport potential. Average critical shear stress profiles, the metric we used for erodibility, were quantified using a power-law fit to cumulative eroded mass vs. shear stress for the flats and channel. Laboratory erosion measurements of deposits made from slurries of flat and channel sediment were used to quantify erodibility over consolidation time scales ranging from 6 to 96 h. Erodibility of the tidal flats was consistently low, with spatial variability comparable to seasonal variability despite seasonal changes in biological activity. In contrast, channel-bed erodibility underwent large seasonal variations, with mobile sediment present in the channel thalweg during winter that was absent in the spring and summer, when channel-bed erodibility was low and comparable to that of the tidal flats. Sediment on the northern (left) channel flank was mobile in summer and winter, whereas sediment on the southern flank was not. Seasonal changes in channel-bed erodibility are sufficient to produce order-of-magnitude changes in suspended sediment concentrations during peak tidal flows. Porosity just below the sediment surface was the best predictor of erodibility in our study area.

1. Introduction

Tidal flats are important coastal sediment storage areas that contribute to the regulation of sediment exchange between terrestrial and marine environments. They are also an important habitat for shore birds, benthic invertebrates and commercially important fish. The residence time of sediment in tidal flat systems, turbidity levels associated with sediment in suspension, and morphological evolution of tidal flats depend in large part on sediment mobility relative to the fluid forcing in the system. For sandy tidal flats, initial motion conditions (e.g., critical shear stress) and settling rates are largely dependent on sediment size and density. For muddy tidal flats, however, mobility is influenced by many additional factors, including consolidation, porosity, flocculation, wetting and drying cycles, organic content, microalgae, macrophytes, invertebrates, and external sediment supply to the system. In temperate settings, many biological processes are most active in summer and input of new sediment to the system accompanies periods of high river discharge in winter, both of which potentially add a seasonal signal to sediment mobility in muddy tidal flat systems.

Owing to the complex biological and physical controls on erodibility of fine-grained (medium silt and finer) sediment, it has not been possible to predict erodibility in the absence of site-specific erosion measurements. A variety of techniques for measuring erodibility of fine-grained sediment have been developed, including in situ flumes (e.g., Widdows et al., 1998; Amos et al., 1992; Maa et al., 1993), erosion chambers (e.g., Gust and Müller, 1997), and water jets (e.g., Tolhurst et al., 1999). Intercomparisons of erosion devices (Gust and Müller, 1997; Tolhurst et al., 2000a; Widdows et al., 2007) reveal considerable variability in entrainment rates and erosion thresholds from device to device. As each erosion device has its positive and negative attributes, no system is clearly superior to the others. In all cases, consistent adherence to established protocols for running erosion tests, as well as minimal disturbance to the sediment column prior to testing, provides the highest quality data (Gust and Müller, 1997; Tolhurst et al., 2000b), and results obtained from similar devices are most comparable (Widdows et al., 2007). We elected to use Gust erosion microcosms (Gust and Müller, 1997) for this study

* Corresponding author. Tel.: +434 924 7546; fax: +434 982 2137.
E-mail address: pw3c@virginia.edu (P.L. Wiberg).

0278-4343/$ - see front matter © 2012 Elsevier Ltd. All rights reserved.
http://dx.doi.org/10.1016/j.csr.2012.07.021

because of our previous experience with the system, physically meaningful results obtained using the system in shallow marine environments (Stevens et al., 2007; Traykovski et al., 2007; Law et al., 2008), and a growing body of results using these erosion microcosms in a range of coastal environments (e.g., Dickhudt et al., 2009; Lawson et al., 2012) that allow for broader comparisons.

Unlike salt marsh-tidal flat complexes common in microtidal environments where marsh vegetation stabilizes the majority of the intertidal landscape, mesotidal environments like those found in Willapa Bay (southwest Washington, USA; Nittrouer et al., 2013) or the German Wadden Sea (e.g., Andersen et al., 2010) can include large expanses of mainly unvegetated intertidal mud flats. As a result, sediment erodibility on the flats is influenced by a variety of factors including sediment and geotechnical properties, seasonal microalgae and other primary producers, presence of complex channel networks, wetting and drying, including rainfall effects, and exchange of sediment between the flats and channels.

The objectives of this study were to quantify erodibility of sediment in a muddy mesotidal flat-channel complex in southern Willapa Bay and its seasonal variations. This is one component of a larger program investigating sediment dynamics and deposition in southern Willapa Bay that includes measurements of sediment grain size (Law et al., 2013), flat porosity and biology (Wheatcroft et al., 2013), flow and suspended sediment (Nowacki and Ogston, 2013; Mariotti and Fagherazzi, 2011; Hill et al., 2013), floc dynamics (Hill et al., 2013), sediment accumulation (Boldt et al., 2013), and geotechnical properties of tidal flat deposits (Barry et al., 2013).

1.1. Site description

This study was conducted in a channel-flat complex at the southeastern end of Willapa Bay, WA (Fig. 1a). This channel-flat complex is part of a series of 4 secondary channels and intervening tidal flats adjacent to Bear River channel and Round Island (Fig. 1b). The channels are identified as AC (northernmost) – DC (southernmost), and tidal flats AF – DF are located just south of the channel with the same letter designation. This study focused on C-Channel (CC) and the flats to the north (B-Flat, BF) and south (C-Flat, CF). CC is about 0.65-km long and the thalweg of the channel is about 1 m below the adjacent tidal flats in the lower reaches of the channel. The elevation of the tidal flats is roughly 0.4 m below MSL. Mean tidal amplitude in the study area is 1.2 m; spring tidal amplitude is about 50% larger than mean amplitude.

Median grain size on the AF-DF flats ranges from 13 to 30 μm with a small sand fraction (~15%) in winter that decreases slightly in summer (Law et al., 2013). Sediment in the channels was generally finer than the flats. Law et al. (2013) found a weak positive correlation of median grain size with elevation and a stronger correlation of decreasing percentage of sediment deposited as flocs vs. single grains with increasing elevation. Average clay fractions in excess of 10% in sediment from the flats and channels in the study area suggest that the sediment in the study area should exhibit cohesive behavior (van Ledden et al., 2004).

Fresh water and sediment is supplied to southern Willapa Bay primarily by the Naselle River, which accounts for about 20% of the total fresh water input to Willapa Bay (Banas et al., 2004). The Naselle River discharge averages 12 $m^3 s^{-1}$, with most of the discharge occurring in the winter months (Nowacki and Ogston, 2013). The closest source of fresh water to the study area is Bear River, a small, ungaged river with a discharge estimated to be 17% of that of the Naselle (Nowacki and Ogston, 2013). Insufficient suspended sediment measurements exist for either the Naselle or Bear Rivers to develop sediment rating curves or estimates of the annual supply of sediment to southern Willapa Bay (Boldt et al., 2013), but the contribution from Bear River is undoubtedly small.

In summer, the flats in the study area are covered with *Zostera japonica*, a small, invasive eelgrass common in the mid-intertidal of Pacific Northwest tide flats (Kaldy, 2006; Wheatcroft et al., 2013). Microalgae also grow on the tidal flats when solar insolation is adequate, primarily in spring and summer. *Spartina*

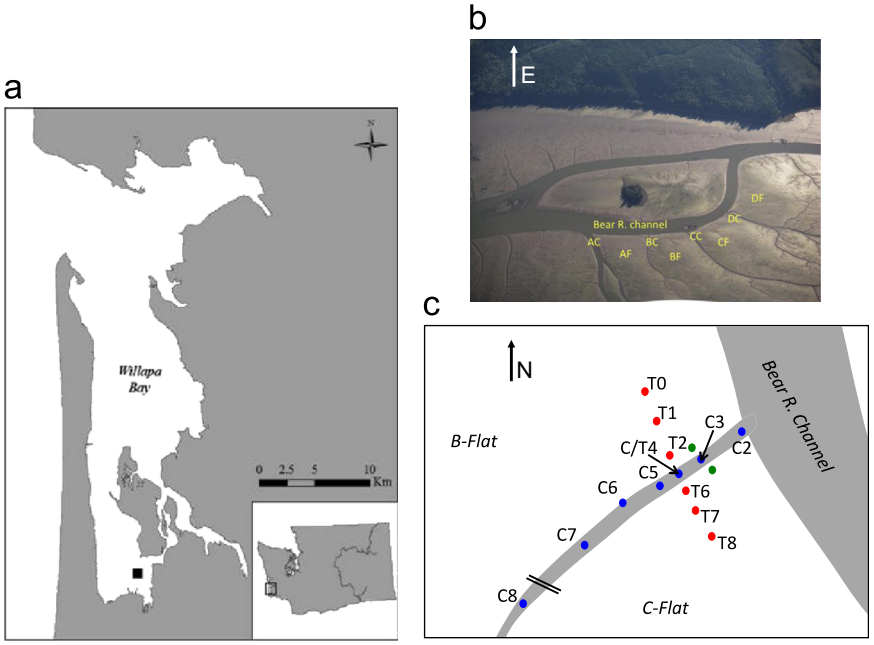

Fig. 1. (a) Location of study area, indicated by black square, in Willapa Bay, WA. (b) Channel-flat complex comprising the study area. This study focused on C-Channel (CC) and adjacent flats, BF and CF. (c) Schematic map of sampling sites along the channel (C-Transect) and transverse to the channel (T-Transect). The numbers correspond to sampling sites, designated C (blue dots) and T (red dots) for sites on the C- and T-Transects, respectively; not shown are sites T3 and T5 on the north (between T2 and T4) and south (between T4 and T6) channel flanks, respectively. The green dots show flat sites along a short transect sampled in March 2009 that also included site C3.

alterniflora, an invasive marsh grass in this system, is largely absent from the tidal flats due to aggressive mechanical and chemical control efforts by Washington State. *Zostera marina*, a native eelgrass, is present in the lower intertidal and subtidal portions of larger channels.

2. Methods

2.1. Field sampling

Three field campaigns were carried out to investigate spatial and seasonal variations in erodibility within C-Channel and the adjacent flats in March 2009, July 2009 and February 2010. In March 2009, samples were collected along a short flat-channel-flat transect centered on channel site C3 (Fig. 1c, green dots). Sampling in July 2009 included a ~350-m-long along-channel transect (C-Transect sites C2–C8, Fig. 1c) as well as several short across-channel transects as in March 2009. The February 2010 sampling concentrated on a ~130-m-long flat-channel-flat transect (T-Transect site T0–T8, Fig. 1c).

At each sampling site, multiple cores were collected from the side of a small boat or kayak using a hand-held corer fit with 10.5-cm-diameter polycarbonate core tubes. The corer recovered 0.3- to 0.6-m-long sediment cores with an undisturbed surface at least 0.1 m below the top of the core tube. The sediment cores and overlying water were capped and returned to a temporary field lab. Two cores from each site were used for erosion testing as described below. The remaining cores were used for measurements of surface grain size (each site) and porosity (most sites).

2.2. Erosion rate measurements

Erosion rates were measured using two Gust erosion chambers (Gust and Muller, 1997; Thomsen and Gust, 2000), 10.7-cm diameter devices that fit on top of a core tube (Fig. 2). The chamber uses a calibrated, rotating upper plate to generate a flow with a specified shear stress on the sediment surface between 0.01 and 0.40 Pa (University of Virginia (UVA) chamber) or 0.01–0.60 Pa (Bedford Institute of Oceanography (BIO) chamber). A flow-through system replaced water pumped out of the chamber with ambient water collected at the sample site; water temperature was allowed to equilibrate to air temperature and remained relatively constant throughout each experiment. In most cases, water leaving the UVA chamber passed through a turbidity sensor that monitored turbidity in NTU (Nephelometric Turbidity Units). Time series of NTU were recorded at 1 Hz in March and July 2009; only intermittent values were recorded in February 2010.

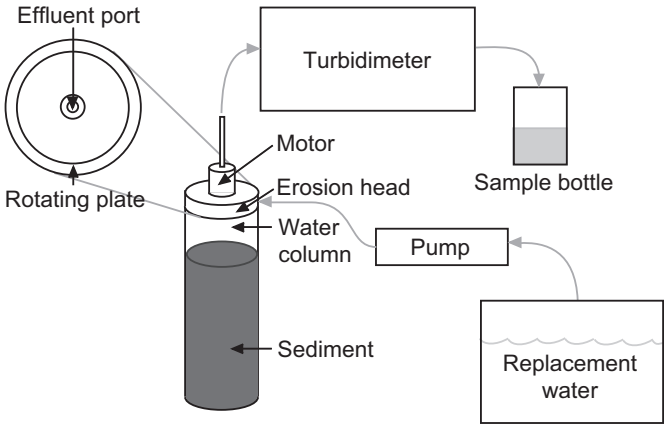

Fig. 2. Schematic of the Gust erosion chamber (Gust and Müller, 1997). The erosion head fits onto a polycarbonate core tube with the sediment surface positioned 0.10 m below the top of the core tube and the head space filled with water. The erosion head includes a rotating plate that generates a flow in the chamber. The rotation rate is calibrated to the shear stress exerted by the flow on the sediment surface. Ambient replacement water is pumped into the chamber at a rate dictated by the specified shear stress, which forces chamber water out through the effluent port, through a turbidimeter and ultimately into a 1–2 L sample bottle. (Following Lawson et al., 2012).

Erosion tests were performed within hours of when each core was collected. Before each experiment began, the sediment surface was raised until it was positioned 10-cm below the core tube top. All erosion tests were run at shear stresses of 0.01 (run as an initializing step and not used in the subsequent analysis), 0.08, 0.16, 0.24, 0.32 and 0.4 Pa; in some tests, shear stresses of 0.48 and 0.60 Pa were also run in the BIO chamber. Beginning with the lowest shear stress, each value of shear stress was maintained for 20 min and then increased. If the applied shear stress exceeded the critical shear stress at the bed surface, turbidity increased quickly and then gradually decreased back toward background conditions as the turbid water was pumped out and replaced with ambient water. The clearing of the water in the erosion chamber while bed shear stress was held constant indicates that all sediment that could be eroded at that shear stress was eroded, leaving a bed with a critical shear stress in excess of the applied stress. In most cases, 20 min was sufficient time for turbidity levels in the erosion chamber to return to near background levels.

Water leaving the chambers was collected in bottles and filtered on pre-weighed Whatcom GF/F glass fiber filters (UVA) or Millipore filters (BIO). UVA filters were dried, combusted and weighed to obtain eroded inorganic sediment mass as the difference between final and initial filter weights. BIO filters were dried at 60 °C and the difference between final filter weight with sediment and initial filter weight was used to calculate total eroded sediment mass. The filters were then placed in a low temperature (<60 °C) oxygen plasma asher to remove the filter and treated with hydrogen peroxide (35%) before inorganic grain size analysis. Eroded mass divided by the volume of water filtered gave average suspended sediment concentration for the time interval during which a water sample was collected. Values of average concentration during each 20-min shear stress interval were used to calibrate the turbidity measurements and convert them to suspended sediment concentration (SSC) time series. The product of SSC ($g\,L^{-1}$) and the rate at which water was pumped through the chamber (L/s) gives the time series of mass erosion rate as a function of time.

Blank filters were used as a check on the accuracy of filter weights. A small but consistently positive value for the final minus initial weight of UVA blanks was noted, and the average increase of 0.003 g/filter was subtracted from UVA filter weights in March 2009 and July 2009; 0.006 g/filter was subtracted from filter weights in February 2010. Subsamples of the effluent from the UVA microcosm analyzed by both UVA and BIO resulted in values of cumulative eroded mass that differed by an average of 4% (rms) in July 2009 and 6% in February 2010. This represents the potential error due to differences and uncertainties in sample processing.

The UVA and BIO erosion chambers were used to measure erosion rates on separate cores for each site. The two erosion chambers were based on the same design. A recent reanalysis of the erosion chamber calibrations that relate the rotation rate of the upper plate to the shear stress applied to the sediment surface (Suttles et al., 2011) indicates that the UVA erosion chamber used a calibration that overestimated the rotation rate required to produce a given shear stress, whereas the BIO chamber used a calibration that underestimated the rotation rate. As a result, the UVA bed shear stresses averaged 2% higher than specified and the BIO bed shear stresses averaged 8% lower than specified. The

relationships between the corrected bed shear stresses and measured cumulative eroded mass (a monotonically increasing function) were used to obtain values of cumulative eroded mass at the intended values of bed shear stress (0.08, 0.16, 0.24, 0.32 and 0.40 Pa). UVA and BIO values of eroded mass at each shear stress were then corrected for the background sediment mass associated with the suspended sediment concentration of the replacement water. UVA and BIO corrected values of cumulative eroded mass as a function of bed shear stress were well correlated (>0.90 correlation coefficient) and showed no significant bias.

This analysis focuses on measurements made at bed shear stresses of 0.08–0.40 Pa, for which eroded mass was measured using both the UVA and BIO erosion chambers. Only UVA measurements are available for March 2009, but duplicate measurements were made at each sampling site. Filter data are missing for one CC and the two CF samples in March 2009, however turbidity time series are available for all erosion tests during that sampling period. Using a turbidity calibration developed for the March CC sample for which both filter data and turbidity time series were available, mass erosion rate time series were calculated using the turbidity time series for the second CC site and the two CF sites, and integrated over each stress step to obtain eroded mass. Comparison of filter data and turbidity time series for the July 2009 samples confirms that the CF and CC turbidity calibrations were similar.

2.3. Supporting measurements

Grain size was determined for surface sediment samples (top few mm) of each core. Samples were disaggregated and treated with hydrogen peroxide (35%) to remove organic material prior to grain size analysis using a Coulter Counter Multisizer IIe as described in Law et al. (2013); results are given in terms of volume concentration (ppm). Similar methods were used to obtain grain size of eroded sediment from subsamples of the water collected during each stress step for a representative set of cores. Porosity profiles were determined from resistivity profiles made in a number of the cores used for erosion testing following the procedure described in Wheatcroft et al. (2013). Monthly values of chlorophyll *a* concentration and eelgrass shoot density on the tidal flats during 2010 are provided in Wheatcroft et al. (2013).

Water surface elevation was measured near the mouth of C-Channel with an RBR TWR-2050 submersible tide and wave logger during 16–28 Jul 2009 and 23 Feb-19 Apr 2010. A second RBR TWR-2050 recorded water elevations and waves on B-Flat during two 3-day periods in Feb–Mar 2010. Aquadopp (Nortek) measurements of pressure in C-Channel (between sites C5 and C6, Fig. 1c) and on B-Flat (Nowacki and Ogstron, 2013) are available for March 2009 (Nowacki and Ogston, personal communication). In all cases, waves were sampled at 4 Hz for 4–12 min every 15 or 30 min and average tidal elevation was recorded at the same intervals. We applied an inverse barometer correction (e.g., Wunsch and Stammer, 1997) to measured water depths to account for the influence of atmospheric pressure on water surface elevation using atmospheric pressure measurements from NOAA's Toke Point station (ID 9440910) near the entrance to Willapa Bay (Fig. 1a; tidesandcurrents.noaa.gov). A further correction was made to account for wave orbital attenuation between the water surface and the depth of the wave logger (Dean and Dalrymple, 1991). Significant wave height was calculated from the variance, m_0, of the corrected surface elevation time series as $H_s=4\,m_0^{1/2}$ (Longuet-Higgens, 1952); wave period was estimated as the peak spectral period and the average zero-crossing period (e.g., Wiberg and Sherwood, 2008). Longer-term records of measured and predicted tides are also available from NOAA's Toke Point station (ID 9440910).

Wind speed and direction and air temperature during the study period were recorded locally by J. Thompson (personal communication), and are also available at Toke Point. Water temperature was recorded at Toke Point. Precipitation data are available from Washington State University's Agronet station in Long Beach, WA. Naselle River discharge was obtained from the USGS (Site 12010000).

2.4. Laboratory experiments

Laboratory measurements of consolidation and erodibility of sediment collected from C-Channel and C-Flat were made using the UVA erosion chamber. Relatively high concentration ($\sim$500 g/L) suspensions of sediment in saline water were allowed to settle in core tubes. During the settling process, we monitored changes in total bulk density and erodibility. Erosion tests were run after 6, 12, 24 and 48 h, and in one case, 96 h of settling and consolidation for bed shear stresses of 0.01, 0.08, 0.16, 0.24 and 0.32 Pa. The laboratory erosion tests were carried out using the same procedures as those outlined above for the field tests.

3. Results

Sites for the erosion tests were selected to capture both spatial and seasonal variations in erodibility for the tidal flats and channel. Results are presented initially to illustrate across- and along-channel variations in erodibility. Seasonal effects are then considered. Values reported for cumulative eroded mass at each shear stress and site represent the average eroded mass for the 2 replicates from each site summed over all shear stresses less than or equal to the specified stress (not including the 0.01 N m^{-2} values) unless otherwise noted.

3.1. Across channel-flat variations in erodibility

Erosion tests were made in February 2010 for samples along the T-Transect, located $\sim$75 m from edge of Bear River Channel (Fig. 1c). Sites T0–T2 were on B-Flat; Sites T3–T5 were on the northern (left) flank, close to the thalweg, and on the southern (right) flank of C-Channel, respectively; Sites T6–T8 were on C-Flat. Erosion tests were run using the UVA and BIO erosion chambers for each of the 9 sites. Average eroded sediment mass (kg m^{-2}) along the T-Transect at applied bed shear stresses, τ_b, from 0.08 to 0.40 Pa is shown in Fig. 3a. Cumulative eroded mass was similar on BF and CF, ranging from 0.005 to 0.034 kg m^{-2} at the maximum bed shear stress of 0.40 Pa. Significantly more sediment, 0.13 kg m^{-2}, was eroded at T4, near the channel center. Cumulative eroded mass at T3 (northern flank) was similar to that measured in the center of the channel, while erosion at T5 (southern flank) was similar to the rest of the CF sites (T6–T8).

Erosion measurements in March 2009 (Fig. 3b) were made along a short flat-channel transect through C3, about 25 m closer to Bear River Channel and roughly in line with sites T2, T4 and T6 (Fig. 1c, green dots). Duplicate erosion tests were run for each site using the UVA erosion chamber. Average cumulative eroded mass on BF and CF was a little higher than in February 2010, ranging from 0.015 to 0.042 m^{-2} at $\tau_b=0.40$ Pa. Erosion in the channel was roughly 50% higher than that on the flats, but significantly lower than measured in February 2010 for stresses >0.16 Pa (Fig. 3c).

Erosion measurements in July 2009 focused on an along-channel transect (Fig. 1c, Fig. 4a). However, several short across-channel transects were also sampled (Figs. 4b and c), one that

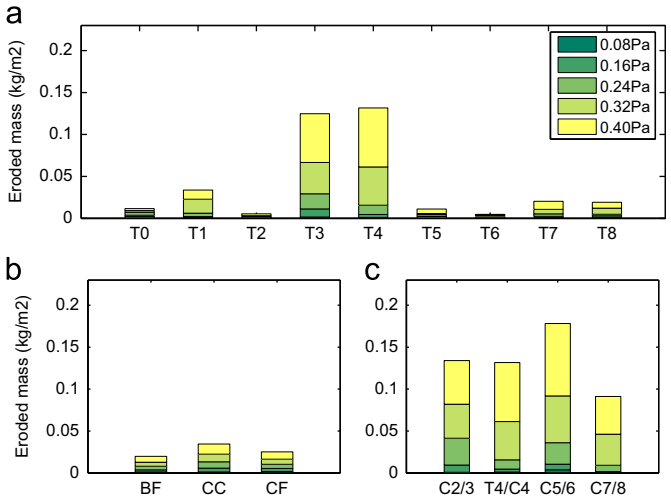

Fig. 3. Measured eroded mass as a function of bed shear stress for sites sampled in February 2010 and March 2009. Each shear stress was maintained for 20 min. Each measurement is the average of 2 replicates. (a) Eroded mass for sites along the T-Transect. (b) Eroded mass along a short channel-transverse transect in March 2009 centered on channel site C3. (c) Eroded mass for sites in the center of C-Channel. Sites between numbered locations in Fig. 1c are designated with the numbered locations on either side, e.g., C2/3 is between C2 and C3. (a) Feb 2010 T-Transect. (b) Mar 2009 C3-Trans and (c) Feb 2010 C-Channel.

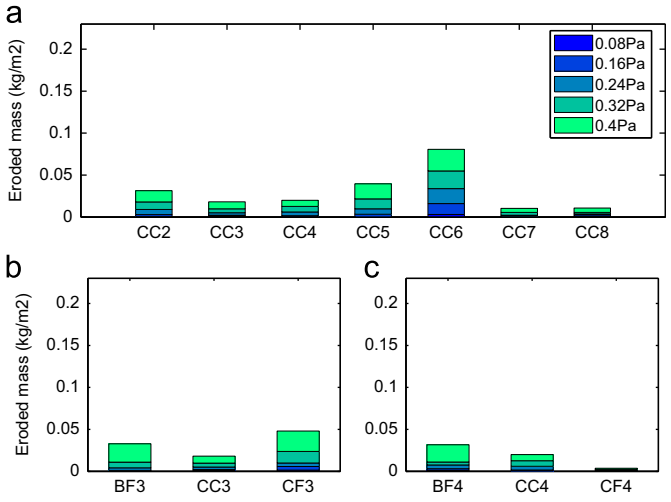

Fig. 4. Measured eroded mass as a function of bed shear stress for sites sampled in July 2009. (a) Eroded mass for sites along the C-Transect. (b) Eroded mass for sites along a short channel-transverse transect centered on channel site C3, as in March 2009 (Fig. 3b). (c) Eroded mass along a short channel-transverse transect comprising sites T2, C4 and T6. (a) July 2009 C-Channel. (b) Jul 2009 C3-Trans and (c) Jul 2009 C4-Trans.

occupied the same sites as the March 2009 measurements (Fig. 1c, green dots) and the other roughly at T2, T4 and T6 (Fig. 1c). Cumulative eroded mass on the flats ranged from 0.004 to 0.048 kg m^{-2} at τ_b=0.40 Pa, similar to values observed in March 2009 and February 2010, with as much within-flat variability between the two transects as there is between flat and channel within each transect.

Differences between average cumulative eroded mass on B-Flat and C-Flat were not significant during any of the sampling periods and are combined in the remainder of this paper.

3.2. Along channel variations in erodibility

Erosion tests were made in July 2009 for samples along the C-Transect, extending from close to the mouth of C-Channel (site C2) to about 350 m up-channel from the edge of Bear River Channel (site C8; Fig. 1c). Erosion tests were run using the UVA and BIO erosion chambers for each of the 7 sites. We attempted to take the cores in the deepest part of the channel, but site C6 was located closer to the channel bank adjacent to B-Flat. Average sediment eroded mass along the C-Transect at bed shear stresses from 0.08 to 0.40 Pa showed no clear trend along the channel (Fig. 4a). Cumulative eroded mass ranged from 0.01 to 0.04 kg m^{-2} at τ_b=0.40 Pa except for site C6, where cumulative eroded mass reached 0.08 kg m^{-2}.

A smaller set of along-channel sites was tested for erodibility in February 2010 (site C4 and sites between C2 and C3 (C2/3), C5 and C6 (C5/6), and C7 andC8 (C7/8); Fig. 3c). Cumulative eroded mass in C-Channel ranged from 0.09 to 0.17 kg m^{-2} at τ_b=0.40 Pa, significantly higher than was observed at all but site C6 in July 2009.

3.3. Seasonal variations in forcing and erodibility

The dominant forcing in the study area is tidal. All sampling periods included peak spring tidal conditions. The maximum tidal range was 3.4–3.5 m in March 2009 and February 2010, and increased to 4.0 m in July 2009 (Table 1). Mean wind speeds were highest in the February 2010 sampling period (2 days averaging 8.4 m s^{-1}), but each sampling period included an interval of higher and one of lower winds, with variable direction (Table 1). Significant wave height was higher in winter (March and February) than summer, but was relatively small in all cases (peak significant wave height $\leq$0.25 m) with wave periods in the range of 1–3 s. The winter sampling periods also were wetter, and river discharge was higher, than summer (Table 1).

Average cumulative eroded mass as a function of shear stress on the tidal flats adjacent to C-Channel was similar during all sampling periods (Table 2). In contrast, channel-bed sediment was much more erodible in February 2010 than in July 2009, excluding Site C6 (Table 2). The differences were modest ($\sim$ factor of 2) but significant at the lower shear stresses, and

Table 1
Forcing conditions during the three sampling periods.

Parameter	Values provided	Mar 2009 (3/10–3/18)	Jul 2009 (7/17–7/28)	Feb 2010 (2/26–3/02)
Wind speed (m s^{-1})/Direction (split into higher and lower wind days)	Day range: Mean (Max) Speed/Dir	10–13: 2.6 (7.1)/187° 14–18: 5.0 (9.8)/277°	17–20: 5.0 (9.8)/82° 21–28: 2.9 (6.5)/106°	26–27: 8.4 (12.6)/186° 2/28–3/2: 2.7 (6.9)/234°
Tide range (m)	Mean (Max)	2.3 (3.4)	2.5 (4.0)	2.7 (3.5)
Significant wave height (m)	Peak (% >0.1 m)	0.25 (6%)	0.19 (1%)	0.25 (13%)
Solar radiation (W m^{-2})	Mean (Max) daily peak	513 (677)	790 (946)	330 (493)
Air temperature (°C)	Mean (Max)	5.2 (11.2)	14.7 (28.7)	9.3 (12.0)
Water temperature (°C)	Mean (Max)	7.2 (8.8)	15.6 (17.9)	9.8 (10.5)
Precipitation (mm)	Total	54	3	26
Naselle R. discharge (m^3 s^{-1})	Mean (Max)	11.6 (19.0)	1.1 (1.2)	13.8 (16.9)

Table 2
Mean cumulative eroded mass as a function of bed shear stress.

Date	Site	Mean cumulative eroded mass (SE) by shear stress, g m^{-2}				
		0.08 Pa	0.16 Pa	0.24 Pa	0.32 Pa	0.40 Pa
Mar 2009†	Flats (2 sites, 4 cores)	1.5 (0.5)	4.5 (1.3)	9.1 (2.5)	14.6 (4.3)	22.5 (7.3)
	Channel (1 site, 2 cores)	1.3	5.8	13.3	22.4	34.5
Jul 2009	Flats (4 sites, 9 cores)	0.7 (0.2)	2.2 (0.5)	5.3 (1.2)	10.0 (2.4)	23.4 (5.6)
	Channel (6* sites, 10 cores)	0.5 (0.1)	2.4 (0.4)	6.4 (1.3)	12.8 (2.6)	21.4 (4.2)
Feb 2010	Flats (7 sites, 14 cores)	1.2 (0.3)	2.7 (0.5)	4.9 (0.7)	9.7 (2.5)	15.1 (3.8)
	Channel (4 sites, 8 cores)	1.6 (0.7)	6.5 (2.1)	25.6 (7.8)	70.3 (10.3)	131 (15.3)

* Site C6 omitted from average (see text). Mean cumulative eroded mass at each stress for C6 was: 3.1, 16, 34, 55, 81 g m^{-2}, respectively.

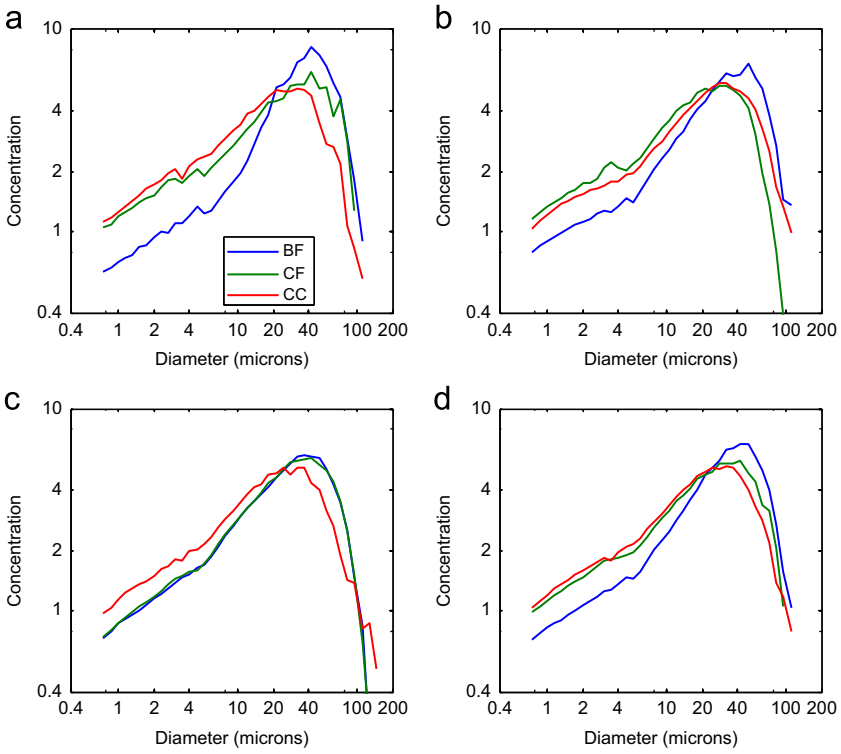

Fig. 5. Disaggregated inorganic grain size (DIGS) distributions for the C-Channel (CC) and adjacent flats (BF and CF) in (a) March 2009, (b) July 2009 and (c) February 2010. (d) The average DIGS distributions over the 3 sampling periods for BF, CC and CF.

but were much more pronounced ($>$ factor of 5) at the higher shear stresses. We made only two measurements of channel-bed erosion in March 2009, but these suggest that the erodibility of this sediment was between that measured in February 2010 and July 2009, and well below the values of cumulative eroded mass at the higher stresses in February 2010.

Comparison of C-Channel Site C6 (July 2009; Fig. 4a) with Site T3 on the T-Transect (February 2010; Fig. 3a), both located on the northern channel flank, suggests that sediment comprising the northern channel flank remained relatively erodible year round. In contrast, the southern channel flank (Site T5) behaved more like the flats.

3.4. Seasonal and spatial variations in bed properties and eroded sediment

Spatial and seasonal variations in erodibility could be expected to be accompanied by variations in porosity and/or surface grain size. Average disaggregated inorganic grain size (DIGS) of the surficial bed material in C-Channel was generally finer than the flats and did not vary much seasonally (Fig. 5, Table 3). The surface of B-Flat was coarser than C-Channel and C-Flat and also appeared to vary little seasonally. CF was more variable, with a grain size distribution similar to that of the channel bed in March and July 2009 but more like BF in February 2010. Sand content, which varied from 5 to 14%, was highest on B-Flat (13%, averaged over all seasons) and in February (12%, averaged over flats and channel). Clay content, which varied from 10 to 19%, was lowest on B-Flat (12%) and in February (14%).

Porosity decreased from an average of 0.75 in the uppermost mm to an average of 0.67 2–4 mm below the surface (Table 3; see also Wheatcroft et al., 2013). In March 2009 and February 2010, porosity was lower on B-Flat than in C-Channel or C-Flat; no spatial variations were apparent in July 2009. In February 2010, bed porosity in C-Channel was higher than on the adjacent flats. Otherwise porosity in CC and CF was similar.

The grain size distribution (in terms of volumetric concentration) of eroded sediment in effluent water collected during each stress step, divided by the size distribution of the bed surface (Fig. 5), provides a measure of the size-specific relative mobility of seabed sediment (Law et al., 2008; Fig. 6). Results from C-Flat (CF) and C-Channel (CC) samples in March 2009 and July 2009 show a common pattern, independent of bed shear stress, of relative mobility >1 for bed fractions <10–20 μm, indicative of water-

Table 3
Average bed sediment grain size and porosity metrics in the study area.

Date	Site	D_{mean} (μm)	Sand %	Silt %	Clay %	Porosity		
						0–1 mm	1–2 mm	2–4 mm
B-Flat	Mar 2009	32	12.9	76.7	10.4	0.72	0.66	0.63
	Jul 2009	31	13.7	73.6	12.7	0.77	0.70	0.66
	Feb 2010	29	12.6	74.5	12.9	0.73	0.67	0.64
C-Channel	Mar 2009	22	7.0	74.2	18.8	0.76	0.71	0.68
	Jul 2009	25	8.7	74.1	17.3	0.72	0.69	0.67
	Feb 2010	26	13.0	71.3	15.7	0.76	0.73	0.71
C-Flat	Mar 2009	25	8.0	74.7	17.3	0.78	0.72	0.69
	Jul 2009	21	4.7	75.9	19.4	0.77	0.70	0.67
	Feb 2010	28	11.2	74.8	14.0	0.74	0.69	0.66

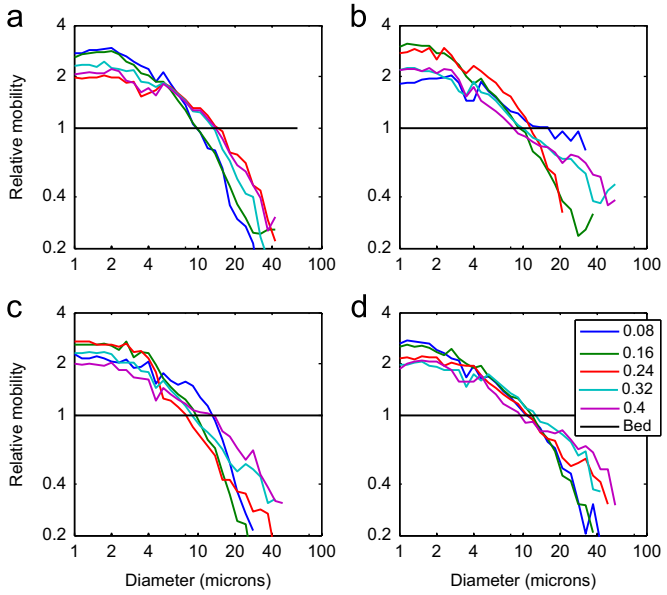

Fig. 6. Size-specific relative mobility, obtained by dividing the disaggregated inorganic grain size (DIGS) distributions for sediment in the effluent water collected during each stress step by the size distribution of the bed surface for C-Flat in (a) March 2009 and (b) July 2009 and for C-Channel in (c) March 2009 and (d) July 2009. The black line at a relative mobility of 1 represents bottom sediments that erode equally from the seabed. Sizes with relative mobilities >1 (<1) are over- (under-) represented in the water column relative to their presence at the bed surface.

column enrichment relative to the bed surface, and relative mobility <1 for the coarser fractions, reflecting their relative absence in the water column compared to the bed surface (Fig. 6). A lack of dependence of relative mobility on bed stress for grain sizes <10–16 μm is characteristic of cohesive bed sediment (Law et al., 2008).

3.5. Laboratory consolidation test

Mass eroded during the laboratory tests showed a clear pattern of reduced erosion with increasing consolidation time over a period of 96 h (Fig. 7). Erosion tests for C-Channel and C-Flat sediment were similar, so results provided here are averages of the two except at 96 h, when only the C-Channel sediment was tested. After 6 h of consolidation, a total of 0.4 kg m^{-2} of sediment was eroded over the course of the erosion test as bed shear stress was increased from 0.08 to 0.32 Pa, the maximum shear stress used in the laboratory tests. At this initial stage of consolidation, the 20 min during which each value of bed shear stress was held constant was not long enough for the suspended sediment concentrations in the erosion chamber to return to background values. Thus the values of cumulative eroded mass are lower bounds. After 12 h, total eroded mass was halved. It more than halved again by 48 and again at 96 h. After 96 h, cumulative eroded mass approached values measured during the field experiments on the flats and for most of the channel samples, except those measured in February 2010. The highest values of cumulative eroded mass measured in C-Channel (February 2010 and northern channel flank in July 2009) were in the range of the 24–48 h consolidation cases in the laboratory tests.

4. Discussion

4.1. Quantifying erodibility

Approaches to quantifying erosion depend on whether sediment deposits exhibit cohesive or noncohesive behavior (e.g., Sanford and Maa, 2001). Three lines of evidence indicate that the sediment on the flats and channel in the study area was cohesive. First, the minimum clay fraction in our samples from BF, CC and CF is 10.4% (Table 3). van Ledden et al. (2004) argued that sediment with clay fractions in excess of 10% exhibit cohesive behavior owing to their geotechnical properties. Second, the initial peak and subsequent decline in suspended sediment concentrations observed in the erosion chamber whenever bed shear stress was sufficient to resuspend bed sediment is characteristic of beds with limited sediment availability, either due to cohesion or armoring. Bed erosion controlled by armoring vs. cohesion can be distinguished by the third line of evidence, size-specific relative mobility of bed sediment (Fig. 6; Law et al., 2008). Armoring-controlled resuspension results in preferential erosion of finer fractions, with progressively larger sediment grains eroded as bed shear stress increases (Wiberg et al., 1994). In contrast, all size fractions up to fine silt are eroded at approximately the same rate in cohesive beds, resulting in relatively constant, positive relative mobility for the finer fractions (<10–16 μm) that is at most weakly dependent on shear stress (Law et al., 2008), similar to that shown in Fig. 6; coarser fractions can show evidence of sorting (Law et al. 2008).

Because of the complex characteristics of fine-grained cohesive sediment, there is no single measure of erodibility that completely captures the response of the sediment to flow. General erosion expressions have the form

$$E = M[\tau_b - \tau_{cr}(z)]^n \quad (1)$$

(Sanford and Maa, 2001), where E is erosion rate, M is an empirical erosion rate constant, τ_{cr} is critical shear stress, z is distance below the sediment surface and n is an empirical exponent. In the simplest case, $n=1$, leaving M and $\tau_{cr}(z)$ to be

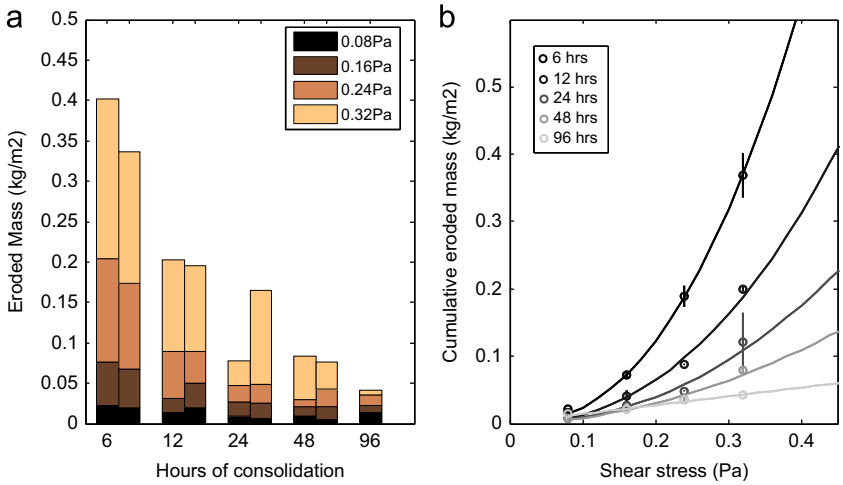

Fig. 7. (a) Measured eroded mass as a function of bed shear stress and hours of consolidation for laboratory consolidation tests. The left and right bars of each pair show values for C-Flat (CF) and C-Channel (CC) sediment, respectively. (b) Cumulative eroded mass as a function of bed shear stress at varying stages of consolidation. Symbols are averages of cumulative eroded mass for the CF and CC consolidation tests; vertical bars show the range of values. The curves are power-law fits to the measurements.

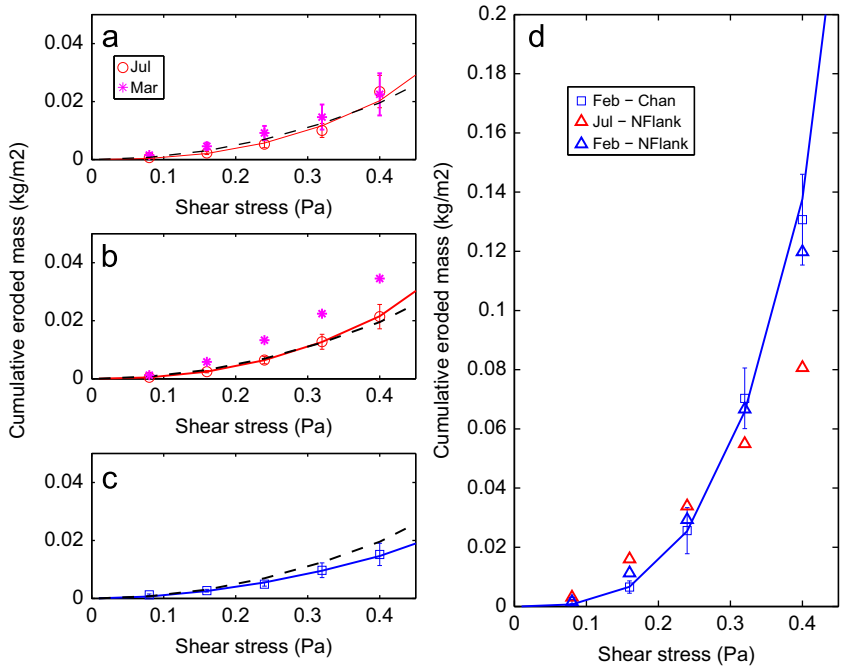

Fig. 8. Cumulative eroded mass (CEM) as a function of bed shear stress. Symbols are averages of cumulative eroded mass for all flat or channel sites at the indicated time; vertical bars show standard error. The curves are power-law fits to the measurements (Table 4). (a) Average for BF and CF, (b) average for CC in March, July 2009. (c) Average for BF and CF and (d) average for CC in February 2010. Triangles in (d) show values for the northern flank of CC in July 2009 and February 2010. The black dashed curve in (a), (b) and (c) is given by CEM=0.126 $\tau_b^{2.03}$.

determined from erosion measurements. Of these, $\tau_{cr}(z)$ is most easily obtained from the erosion measurements presented here. If we assume that all sediment at the bed surface having a critical shear stress less than the applied stress is eroded during the first 20 min at a particular stress, then the remaining bed-surface sediment must have a critical shear stress greater than or equal to the applied shear stress. Cumulative eroded mass as a function of applied bed shear stress (Fig. 8) can then be recast as critical shear stress as a function of cumulative eroded mass. If the density and porosity of the eroded sediment are known, then cumulative eroded mass can be converted to equivalent depth, yielding a depth profile of critical shear stress. It is worth noting, however, that for many sediment transport calculations, it is at least as useful to quantify critical shear stress as a function of eroded mass (and hence mass of sediment added to suspension) as it is to quantify critical shear stress as a function of depth below the bed surface, in which case sediment density and porosity must be specified to convert erosion depth to suspended mass. Time series of mass erosion rate, E, obtained from the calibrated turbidity time series and water pumping rates, together with the critical shear stress profile, allow M to be calculated using Eq. (1).

In many coastal and marine environments, the critical shear stress for muddy sediment increases rapidly with depth into the sediment bed, reaching relatively high values within millimeters of the bed surface. In these environments, sediment resuspension can be strongly supply limited. That is, the capacity of the flow to maintain sediment in suspension can greatly exceed the mass of sediment available to be suspended. For a well consolidated bed, the mass of sediment in suspension during an interval of constant or moderately increasing bed shear stress is more likely to be

controlled by the rate at which critical shear stress increases with depth than by the rate at which sediment can be entrained into the water column. The reverse could be true under conditions of very large and rapid increases in bed shear stress or relatively thick new deposits of unconsolidated fine sediment. Quantifying erosion rates is complicated by the pronounced variations in rates that occur during erosion of cohesive beds. Erosion rates are highest immediately after an increase in shear stress and decrease thereafter as the supply of available sediment becomes exhausted. As a result, any constant value of erosion rate ascribed to a given flow condition is necessarily a function of the time over which the erosion rate is averaged. This makes it difficult to compare erosion rates measured in different studies and contributes to uncertainty in reported values of sediment erodibility (Sanford, 2005).

Even in relatively well consolidated sediment, where erodibility is primarily controlled by $\tau_{cr}(z)$, there is no single "critical shear stress" value that can quantify erodibility. A threshold value of shear stress can be defined, e.g., the shear stress needed to increase suspended sediment concentrations (SSC) above some threshold value (Widdows et al., 2000; Tolhurst et al., 2000a), but there is no broad agreement on what such a threshold value of SSC should be. Furthermore, selecting a single threshold value of critical shear stress neglects the important control that the rate of increase in critical shear stress with depth below the sediment surface exerts on the mass of sediment eroded from the bed in response to a flow. In contrast, under supply-limited conditions, quantifying the critical shear stress profile allows the mass of erodible sediment to be estimated for a given bed shear stress, at least up to the maximum shear stress for which erosion tests were made.

4.2. Tidal flat and channel erodibility in southern Willapa Bay

The relatively rapid rates of consolidation observed in our laboratory measurements (Fig. 7), in addition to daily wetting and drying of the tidal flats, suggest that tidal flats in the study area were well consolidated. This expectation was borne out in the erosion tests for our tidal flat sites and supported by in situ porosity profiles (Wheatcroft et al., 2013). In our erosion tests, bed shear stress increased from 0 to 0.4 Pa over a 2 h interval, comparable to rates observed during flooding tides in channels and on flats during the study (Nowacki and Ogston, 2013; Mariotti and Fagherazzi, 2011). An average of 15–23 g m^{-2} of sediment was resuspended from the tidal flat sites we sampled (Table 2, Fig. 8), equivalent to the uppermost few tenths of a millimeter of the sediment bed. For all stresses that produced resuspension of tidal flat sediment in our tests, the supply of erodible sediment was generally exhausted by the end of the 20-min during which each stress was held constant. We conclude from our results that resuspension and transport of tidal flat sediment in southern Willapa Bay is supply limited (in the sense that the flow could maintain more sediment in suspension than is available at the bed surface at a given bed shear stress) and erodibility is primarily controlled by the rate of increase of critical shear stress with depth below the bed surface (Fig. 8) rather than the rate at which sediment can be entrained from the surface.

Channel bed sediment displayed a wider range of erodibility than the flats, with cumulative eroded mass ranging from values comparable to those for the flats to values that are more than five times larger (Table 2, Fig. 8). There was no discernable trend in along-channel erodibility (Figs. 3c and 4a). In February 2010, when the channel-bed was most erodible, 1–2 mm of the bed was eroded over the course of the erosion tests. Comparison with the laboratory consolidation tests (Fig. 7) indicates that the channel bed sediment surface behaved as though it was partially, but not completely, consolidated. This could be the result of relatively frequent suspension and re-deposition of channel bed sediment during winter conditions. The critical shear stress profile for the February 2010 channel bed is similar to one found by Dickhudt et al. (2009), also using a Gust erosion microcosm, for their "low" erodibility (mostly summer and fall) samples in the York River, a sub-estuary of Chesapeake Bay. The Dickhudt et al. (2009) "high" erodibility sites in the York River were almost an order of magnitude higher than the high erodibility samples from C-Channel.

Table 4
Slopes and intercepts of power-law fits to erosion measurements *.

Date	Site	Slope (SE)	Intercept (SE)	r^2
Mar 2009†	Flats	1.73 (0.032)	−2.23 (0.044)	0.999
	Channel	1.94 (0.034)	−1.58 (0.047)	0.999
Jul 2009	Flats	2.50 (0.239)	−1.61 (0.328)	0.982
	Channel	2.37 (0.010)	−1.67 (0.014)	1.00
Feb 2010	Flats	1.92 (0.133)	−2.47 (0.182)	0.991
	Channel	3.30 (0.089)	1.04 (0.122)	0.999
All Flats		2.03 (0.224)	−2.07 (0.307)	0.892

* Fits to cumulative eroded mass (CEM) as a function of bed shear stress (τ_b) have the form CEM = exp (Intercept) * τ_b^{Slope}.

Average critical shear stress profiles for the flats and channel were quantified using a power-law fit to cumulative eroded mass vs. shear stress (Sanford and Maa, 2001; Dickhudt et al., 2009). Slopes and intercepts of the power-law fits to average cumulative eroded mass on the flats for the three sampling periods do not differ significantly from the overall average values for the flats (Table 4). The average power-law relationship for the flats is CEM = 0.126 $\tau_b^{2.03}$, where CEM = cumulative eroded mass. Channel-bed erodibility in July 2009 is also well described by this relationship (Fig. 8). In March 2009, channel-bed values of cumulative eroded mass were more than 60% larger than in July, but the sample size in March was too small to determine whether these differences were significant. The average power-law relationship for the channel bed in February 2010, the sampling period when the bed was most erodible (Table 2, Fig. 8), is CEM = 2.83 $\tau_b^{3.30}$; the slope and intercept are significantly greater than we observed for the channel at any other time or for the flats at any time (Table 4).

The northern channel flank appeared to be persistently more erodible than the southern channel flank or the tidal flats (Fig. 8). This was also evident during field data collection, when the northern channel flank was not able to support a person walking on the surface without sinking in. [We only walked on the flat following sampling or well away from sampling sites.] A visual survey of the channel banks in the area revealed that the channels flanks sometimes contained slumps. The year-round presence of slump features along the channel banks, with overlying finely laminated deposits, was also observed in x-radiographs of channel-bank cores (Boldt et al., 2013). Rapid infill above slump blocks may contribute to the high erodibility and low bearing strength of the northern channel flanks. Groundwater seepage (Le Hir et al., 2000; Rinehimer et al., 2013) could also help to maintain high erodibility on the channel flank.

4.3. Relationship to porosity and grain size metrics

Spatial variability in the mass of sediment eroded on the tidal flats and within the channel could be influenced by the variations in grain size and porosity observed within the study area (Law et al., 2013; Wheatcroft et al., 2013). A regression analysis revealed that three parameters, porosity 1–2 mm below the bed surface, porosity 2–4 mm below the bed surface and floc fraction,

the percentage of material deposited on the seabed in flocs (Law et al., 2013; Curran et al., 2004), were significantly correlated with total eroded mass in February 2010 ($p < 0.05$). The best correlations for total eroded mass were with porosity 2–4 mm below the surface ($r^2 = 0.67$) and floc fraction ($r^2 = 0.78$) (Fig. 9). Law et al. (2013) found a significant correlation between porosity 2–4 mm below the surface and floc fraction.

Total eroded mass at sampling sites in March and July 2009 was not significantly correlated with any measure of grain size or porosity at those sites. When these are added to the February 2010 values, however, the correlations with porosity 2–4 mm below the surface and with floc fraction (Fig. 9) remain significant, although values of r^2 become smaller (0.29 and 0.32, respectively). The slopes of power-law fits to cumulative eroded mass vs. bed shear stress for individual sampling sites were not significantly correlated with porosity or grain size metrics for any sampling period.

We also considered whether channel- and flat-averaged total eroded mass (Table 2) or the slopes and intercepts of power-law fits to average cumulative eroded mass vs. bed shear stress (Table 4) during the 3 sampling periods were significantly correlated with average porosity or grain size metrics (Table 3). The slopes and intercepts of the power-law fits were significantly correlated with average porosity 2–4 mm below the surface (Fig. 10), as was average total eroded mass ($r^2 = 0.85$; not shown). When the results for the 2 cores from the northern channel flank (one in July 2009, the other in February 2010) were added to the regression (* in Fig. 10), the relationships between power-law slopes and intercepts and porosity 2–4 mm below the surface remained significant (Fig. 10), while the relationship between total eroded mass and porosity was no longer significant. Thus, average porosity just below the sediment surface was the best predictor of the average erodibility of tidal flat, channel bed, and channel flank sediment in our study area.

4.4. Seasonal patterns

Two notable conclusions are suggested by our results regarding the seasonal behavior of erodibility in the mesotidal, muddy flat-channel complex we investigated in southern Willapa Bay. The first is related to the lack of seasonal variability in erodibility

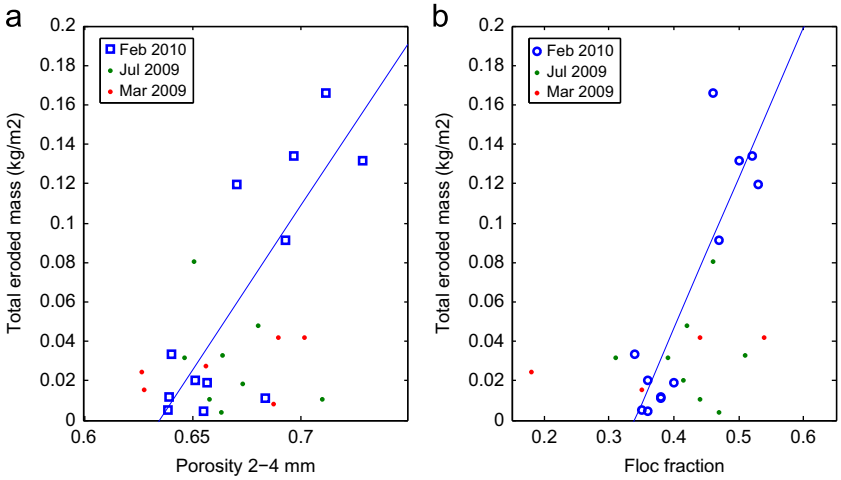

Fig. 9. Correlation between total eroded mass during the erosion tests and (a) porosity 2–4 mm below the sediment surface and (b) floc fraction at the sediment surface. Both correlations are significant for the February 2010 values alone and for the full set of values during all three sampling periods.

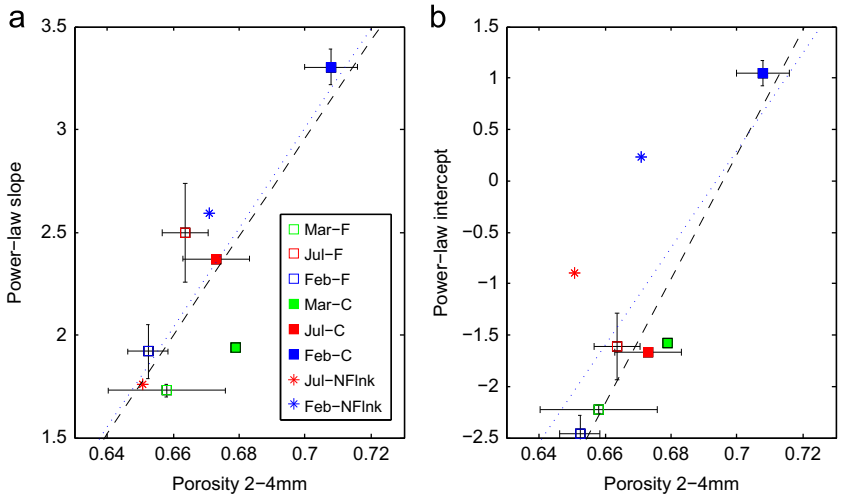

Fig. 10. Correlation between average porosity 2–4 mm below the sediment surface (P24) (Table 3) and the (a) slopes (PLS) and (b) intercepts (PLI) of power-law fits to average cumulative eroded mass vs. bed shear stress (Table 4). Both correlations are significant ($p < 0.05$). The horizontal and vertical bars show standard error for each parameter, with the exception of C-Channel in March 2009 (Mar-C) and the northern channel flank in July 2009 and February 2010 (Jul-NFlnk and Feb-NFlnk) for which values for only one sampling site are available. The regressions equations (dashed lines) for the flat and channels averages are PLS = 23.9 × P24 − 13.8 ($r^2 = 0.69$) and PLI = 60.7 × P24-42.4 ($r^2 = 0.92$). The dotted regression lines, which include the channel flank sites as well, are also significant, with $r^2 = 0.69$ for PLS and $r^2 = 0.52$ for PLI.

of the tidal flats, despite their exposure to seasonal changes in air temperature, solar radiation, precipitation and wave conditions (Table 1) and seasonal differences in biological activity (Wheatcroft et al., 2013). The second is the strong seasonality in the erodibility of channel-bed sediment.

The appearance of the tidal flats in the study area changed markedly between our three sampling periods. In March 2009, the coldest and wettest of the sampling periods (Table 1), the flats were mostly unvegetated (1 CF core included a few *Z. japonica* blades) and we did not note any widespread microalgae on the sediment surface. In July 2009, the warmest, driest and sunniest sampling period, the flats were generally covered with *Z. japonica* although the density was sparse enough that some cores contained stems while others did not. In February 2010, the flats had only a few remnant *Zostera* stems on the surface. There was, however, a visible layer of diatoms on much of the flat surface, giving the flats a rusty-colored tinge. This is consistent with monthly measurements of shoot density on C-Flat and D-Flat during 2010 (Wheatcroft et al., 2013) that showed low densities ($\sim$20 shoots m^{-2}) through the winter and early spring, that increase by an order of magnitude in summer and early fall. Chlorophyll *a* concentrations in 2010 were variable, averaging roughly 20 $\mu g\ g^{-1}$ (Wheatcroft et al., 2013).

Despite the biological changes we observed on the tidal flats, none of the surface grain size characteristics of B- and C-Flat (Table 3) differed significantly with season, nor did the relative mobility of the bed surface (Fig. 6). Porosity near the surface was significantly higher in July 2009 than February 2010, but neither was significantly different than values measured in March 2009. At low bed shear stresses (0.08–0.24 Pa), cumulative eroded mass was significantly larger in March 2009 than in July 2009, but those differences became insignificant at stresses of 0.32–0.40 Pa (Table 2). March 2009 values were also larger than in February, but these differences were not significant for the most part; July 2009 and February 2010 flat values also were not significantly different. These results indicate that biological processes were not the dominant control on tidal flat erodibility in our study area, in contrast to results found in some other muddy tidal flat systems (e.g., Widdows et al., 2000; Andersen et al., 2010). A lack of seasonal variation was also observed in x-radiographs of cores from the flats in summer and winter, which were primarily characterized by bioturbated structures (Boldt et al., 2013). In general, there was as much spatial variability in erodibility within the flats during each sampling period as there was temporal difference between sampling periods.

The channel-bed was considerably more erodible in February 2010 than it was in either March 2009 or July 2009. In July 2009, channel bed erodibility did not differ significantly from that of the flats, suggesting the channel bed was well consolidated. This is supported by x-radiographs of channel-bed cores collected in C- and D-Channels in July 2009 (Boldt et al., 2013), which showed a surface layer of shell hash overlying consolidated, unlaminated sediment. In contrast, channel-bed cores collected in C- and D-Channels in March 2009 and January/February 2010 had a 15-30 cm-thick upper, laminated section overlying a layer of shell debris in many cases (Boldt et al., 2013). In addition, ^{7}Be was present at the surface of the winter channel-bed cores, but was absent from channel-bed cores collected in summer (Boldt et al., 2013). This suggests a fluvial source for the sediment comprising the winter laminated channel-bed deposit (Boldt et al., 2013).

The core x-radiographs suggest that the more erodible channel-bed sediment in February 2010 was a seasonal deposit that is absent in summer. While channel-bed x-radiographs from March 2009 also indicate the presence of a surficial laminated deposit, our channel-bed cores from that sampling period (Site C3, Fig. 1c) were not as erodible as channel-bed samples from February 2010 (Figs. 3 and 4). Only 1 channel site was sampled in March 2009, so we don't have a very complete picture of the channel bed at that time. However, the clay content at the March 2009 channel-bed site was above, and the sand content was below, confidence intervals around mean values for both July 2009 and February 2010. Porosity 2–4 mm below the channel-bed surface in March 2009 was similar to July 2009, which was significantly smaller than in February 2010. Thus the finer but more consolidated (based on porosity) channel bed in March 2009 compared to February 2010 may explain the lower erodibility observed in March.

4.5. Sediment transport potential

If we assume that the mass of sediment available for resuspension at any time is supply limited and controlled by the relationship between bed shear stress and measured cumulative eroded mass (Fig. 8), as suggested by our results, then we can use these relationships to make simple estimates of suspended sediment concentration (SSC) under given flow conditions (bed shear stress and water depth), provided we also assume that the flow and bed conditions are quasi-uniform. Resulting estimates of SSC can be compared with measured (Nowacki and Ogston, 2013; Hill et al., 2013; Mariotti and Fagherazzi, 2011) values of SSC in secondary channels and adjacent flats in the study area.

Water-column observations indicate that the highest velocities and SSC in C-Channel occur during ebb and flood tide pulses that happen when water elevation is about 0.1–0.2 m above the level of the flats (water depths of 1.0–1.2 m in the channel) (Nowacki and Ogston, 2013; Hill et al., 2013). Shear velocities (combined wave and current, u^{*wc}) during the pulses were in the range of $0.01 - < 0.03\ m\ s^{-1}$ with little seasonal variation (Nowacki and Ogston, 2013). A mid-range value of $u^{*wc} \approx 0.02\ m\ s^{-1}$, equivalent to a bed shear stress $\tau_b \approx 0.4$ Pa, yields an available sediment mass for suspension of 0.13 $kg\ m^{-2}$ for the February 2010 channel conditions and 0.02 $kg\ m^{-2}$ for the channel bed under summer conditions and for the flats year round. For a channel depth of 1.0 m, and assuming a well-mixed water column (consistent with small ratios of settling velocity to shear velocity), this gives an average SSC of 0.13 g/L for C-Channel during February 2010 conditions and $\sim$0.02 g/L for July 2009 conditions. Nowacki and Ogston (2013) note background concentrations $\sim$0.01 g/L in C-Channel in July 2009. The overall low erodibility of the flats and channel at that time suggest that concentrations are generally unlikely to greatly exceed background levels during summer conditions, although the more erodible northern channel flank could serve as a potential source for larger volumes of suspended sediment.

Our estimated of SSC for February 2010 is near the lower bound of measured near-bed SSC in C-Channel at bed shear stresses of 0.4 Pa in December 2009 (Nowacki and Ogston, 2013); median near-bed of SSC was about 0.5 g/L during ebb and flood tide pulses in December 2009, quite a bit higher than our erosion tests indicate could have been supplied by resuspension if erodibility in December 2009 was similar to that in February 2010. The discrepancy suggests that the channel bed may have been more erodible in December 2009 than in February 2010, that there may have been convergence in sediment flux that increased SSC relative to values expected under uniform conditions, or that this approach for estimating SSC, which ignores small-scale spatial heterogeneity and details of the turbulent flow and particle dynamics, is too simplistic. All are possible. Water-bottle measurements of SSC in C-Channel showed a 6-fold decrease in peak concentrations (3.2 to 0.5 g/L) between samples collected in early January and February 2010 (Boldt et al., 2013), and Hill et al. (2013) measured SSC values of $\sim$0.06 g/L during the

flood and ebb tide pulse during spring tide conditions in C-Channel in February 2010. These observations suggest that the channel bed was more erodible earlier in the winter than it was during our February 2010 erosion tests, perhaps due to higher river (and sediment) discharge, wind conditions and rainfall (Boldt et al., 2013; Nowacki and Ogston, 2013) in late December 2009—early January 2010. With respect to sediment flux convergence, Mariotti and Fagherazzi (2011) concluded that advection of sediment from other areas of Willapa Bay contributed to peak SSC during flood tides measured in a nearby channel-flat complex. Finally, recent studies by Letter and Mehta (2011) and Son and Hsu (2011) underscore the complex nature of cohesive sediment dynamics near the sediment-water interface. Our estimates, while incorporating some of that complexity (depth variation of critical shear stress), are based on very simplified characterizations of flow and sediment dynamics. Nevertheless, this simple approach to estimating sediment availability has yielded reasonably good results in other applications (e.g., Traykovski et al., 2007).

If the early winter channel bed resembled the deposits that consolidated for 6–12 h in our laboratory tests (Fig. 7), resuspension of bed sediment having a critical shear stress of 0.4 Pa or less could supply sufficient sediment to bring average SSC up to 0.5 g/L during the flood or ebb pulse. These consolidation time scales would be consistent with a high porosity, mobile channel bed undergoing tidal suspension and redeposition. The progressive decrease in erodibility and near-surface porosity through the course of the winter and spring suggested by our measurements implies that the channel bed became increasingly consolidated. Gradual removal of a seasonal, consolidating deposit overlying a well consolidated, longer-term channel floor could explain our observed trends in erodibility and porosity at the bed of C-Channel.

4.6. *Implications for exchange between channels and flats*

Boldt et al. (2013) have proposed a conceptual model of the seasonal cycle in tidal channel-flat complexes in southern Willapa Bay in which sediment accumulates in the channel bed during winter when fluvial sediment discharge into southern Willapa Bay is highest and the flats lack halophytic or microalgal coverings. This sediment is redistributed onto the tidal flats in spring and summer when the presence of eelgrass and microalgae increases the trapping efficiency of the flats, leaving a highly consolidated bed covered with shell debris at the channel bottom during the summer.

Our erosion data support this conceptual model. In the winter, sediment erodibility is much higher in the channels than on the flats, resulting in high SSC within the channel during peak tidal bed shear stresses. The higher SSC channel water is transported onto the flats during flood tides, but net deposition on the flats appears to be minimal in winter. Hill et al. (2013) argue that during spring flood tides, flocculated sediment in suspension in the channels is advected onto the flats, some of which deposits on the channel banks and fringing flats. However, most of the sediment deposited on the flats is removed by ebbing flows and transported back to the channel (Hill et al., 2013).

In spring and summer, sediment erodibility, and therefore SSC, is low on the flats and in the channel. Eelgrass stems and microalgae on the flats can aid in trapping any sediment that is deposited on the flats. Average sediment accumulation rate on the flats is 1.4 mm/yr (Boldt et al., 2013), which roughly balances the amount of sediment stored in the channels during winter conditions (Boldt et al., 2013). This suggests that deposition on the flats begins in late winter/early spring when biological activity on the flats increases, and continues until the volume of fluvially supplied sediment, temporarily stored in the channels during winter, is exhausted. This deposition does not appear to significantly increase erodibility on the flats, likely due to biological stabilization during spring and summer. Drainage and desiccation of the flats when they are exposed during low tides may also facilitate rapid consolidation of any newly deposited sediment.

5. Conclusions

Summer and winter measurements of erodibility and related sediment characteristics in a muddy mesotidal flat-channel complex in southern Willapa Bay, WA, revealed that the tidal flats were well consolidated and characterized by persistently low erodibility despite significant seasonal variations in biological activity on the flats. The bed of the secondary tidal channel adjacent to the flats exhibited relatively high erodibility in winter and low erodibility, comparable to that of the flats, in summer. These seasonal changes in channel-bed erodibility are sufficient to produce order-of-magnitude changes in suspended sediment concentration during peak tidal flows in the channel. Comparison with laboratory measurements of erodibility and consolidation suggests that high winter channel-bed erodibility is associated with a partially consolidated bed. The channel flanks mediate the exchange of sediment between the channel and flats and, at least in some locations, maintain relatively high erodibility year round.

Average critical shear stress profiles, the metric we used for erodibility, were quantified using a power-law fit to cumulative eroded mass vs. bed shear stress for the flats and channel. Total eroded mass during the erosion tests and the power-law fits were both significantly correlated with measured near-surface bed porosity (2–4 mm below the sediment surface). The resulting quantitative relationships among bed shear stress, eroded sediment mass, and porosity provide important constraints on sediment availability in models of tidal flat morphodynamics, and indicate that suspended sediment concentrations and fluxes on tidal flats can be strongly supply limited owing to consolidation and cohesion of tidal flat sediment when average clay content is 10% or higher.

Our results lend support to a conceptual model of mesotidal channel-flat sediment exchange in southern Willapa Bay that was developed based on water column measurements and analysis of sedimentary deposits (Boldt et al., 2013; Nowacki and Ogston, 2013). The conceptual model argues for a temporary accumulation of fluvially supplied, mobile sediment in the channels in winter that is gradually redistributed into the tidal flats during the late winter and spring when biological activity increases sediment retention on the flats.

Acknowledgements

This study was funded by the Office of Naval Research grants N00014-07-1-0926 (PW), N00014-10-1-0305 (BL and TM) and N00014-10-0248 (RW). We thank Chuck Nittrouer, Andrea Ogston, Katie Boldt, and Dan Nowacki for their help with field logistics and John Newgard, Sean McLoughlin, Allison Leach, Aryn Hoge, Jessica Carriere-Garwood, Vanessa Page and Margaret Bjoring for their help with sample collection, erosion testing and other aspects of this study. This paper was improved by the comments of two anonymous reviewers.

References

Amos, C.L., Grant, J., Daborn, G.R., Black, K.S., 1992. Sea Carsousel—a benthic annular flume. Estuarine, Coastal and Shelf Science 34, 557–577.

Andersen, T.J., Lanuru, M., van Bernem, C., Pejrup, M., Reithmueller, R., 2010. Erodibility of a mixed mudflat dominated by microphytobenthos and Cerstoderma edule, East Frisian Wadden Sea, Germany. Estuarine Coastal and Shelf Science 87, 197–206.

Banas, N.S., Hickey, B.M., MacCready, P., Newton, J.A., 2004. Dynamics of Willapa Bay, Washington: a highly unsteady, partially mixed estuary. Journal of Physical Oceanography 34, 2413–2427.

Barry, M., Johnson, B., Law, B., Boudreau, B., Wheatcroft, R., Page, V., Hill, P., 2013. Sedimentary and geo-mechanical properties of Willapa Bay tidal flats. Continental Shelf Research 60S, S198–S207.

Boldt, K.V., Nittrouer, C.A., Ogston, A.S., 2013. Seasonal transfer and net accumulation of fine sediment on muddy tidal flat: Willapa Bay, Washington. Continental Shelf Research 60S, S157–S172.

Curran, K.J., Hill, P.S., Schell, T.M., Milligan, T.G., Piper, D.J.W., 2004. Inferring the mass fraction of floc-deposited mud: application to fine-grained turbidites. Sedimentology 51, 927–944.

Dean, R.G., Dalrymple, R.A., 1991. Water Wave Mechanics for Engineers and Scientists. World Scientific, Singapore 353pp.

Dickhudt, P.J., Friedrichs, C.T., Schaffner, L.C., Sanford, L.P., 2009. Spatial and temporal variation in cohesive sediment erodibility in the York River estuary USA: a biologically influences equilibrium modified by seasonal deposition. Marine Geology 267, 128–140.

Gust, G., Müller, V., 1997. Interfacial hydrodynamics and entrainment functions of currently used erosion devices. In: Burt, N., Parker, R., Watts, J. (Eds.), Cohesive Sediments. John Wiley and Sons Ltd, pp. 149–174.

Hill, P.S., Newgard, J.P., Law, B.A., Milligan, T.G., Linking suspended floc dynamics to the spatial distribution of sediment texture on the Shoalwater Bay tidal complex in Willapa Bay. Continental Shelf Research, this volume.

Kaldy, J.E., 2006. Production ecology of the non-indigenous seagrass, dwarf eelgrass (*Zostera japonica* Ascher. & Graeb.), in a Pacific Northwest Estuary. USA. Hydrobiologia 553, 201–217.

Law, B.A., Hill, P.S., Milligan, T.G., Curran, K.J., Wiberg, P.L., Wheatcroft, R.A., 2008. Size sorting of fine-grained sediments during erosion. Continental Shelf Research 28, 1935–1946.

Law B.A., Milligan, T.G., Hill, P.S., Newgard, J., Wheatcroft, R.A.,Wiberg, P.L., Bed Flocculation on a muddy intertidal flat in Willapa Bay, Washington, Part I: A regional survey of the grain size of surficial sediments. Continental Shelf Research, this volume.

Lawson, S.E., McGlathery, K.J., Wiberg, P.L., 2012. Enhancement of sediment suspension and nutrient flux by benthic macrophytes at low biomass. Marine Ecology Progress Series 448, 259–270.

Le Hir, P., Roberts, W., Cazaillet, O., Christie, M., Bassoullet, P., Bacher, C., 2000. Characterization of intertidal flat hydrodynamics. Continental Shelf Research 20, 1433–1459.

Letter, J.V., Mehta, A.J., 2011. A heuristic examination of cohesive sediment bed exchange in turbulent flows. Coastal Engineering 58, 779–789.

Longuet-Higgens, M.S., 1952. On the statistical distribution of the heights of sea waves. Journal of Marine Research 11, 245–266.

Maa, J.P.-Y., Wright, L.D., Lee, C.H., Shannon, T.W., 1993. VIMS Sea Carousel—a field instrument for studying sediment transport. Marine Geology 115, 271–287.

Mariotti, G., Fagherazzi, S., 2011. Asymmetric fluxes of water and sediments in a mesotidal mudflat channel. Continental Shelf Research 31, 23–36.

Nittrouer, C.A., Raubenheimer, B., Wheatcroft, R.A., 2013. Lessons learned from comparison of mesotidal sand- and mudflats. Continental Shelf Research 60S, S1–S12.

Nowacki, D.J., Ogston, A.S., 2013. Water and sediment transport of channel-flat systems in a mesotidal mudflat: Willapa Bay, Washington. Continental Shelf Research 60S, S111–S124.

Rinehimer, J.P., Thomson, J., Chickadell, C.C., 2013. Thermal observations of drainage from a mud flat. Continental Shelf Research 60S, S125–S135.

Sanford, L.P., 2005. Uncertainties in sediment erodibility estimates due to a lack of standards for experimental protocols and data interpretation. Integrated Environmental Assessment and Management 2, 29–34.

Sanford, L.P., Maa, J.P.-Y., 2001. A unified erosion formulation for fine sediments. Marine Geology 179, 9–23.

Son, M., Hsu, T.-J., 2011. The effects of flocculation and bed erodibility on modeling cohesive sediment resuspension. Journal of Geophysical Research 116, 18.

Stevens, A.W., Wheatcroft, R.A., Wiberg., P.L., 2007. Seabed properties and sediment erodibility along the western Adriatic margin, Italy. Continental Shelf Research 27, 400–416.

Suttles, S. L.P. Sanford and P.J. Dickhudt, 2011. Review, analysis and recommendations for application of operational calibrations for UMCES-Gust erosion microcosm systems (U-GEMS). Informal Report, UMCES.

Thomsen, L., Gust, G., 2000. Sediment erosion thresholds and characteristics of resuspended aggregates on the western European continental margin. Deep-Sea Research Part 1 (47), 1881–1897.

Tolhurst, T.J., Black, K.S., Shayler, S.A., Mather, S., Black, I., Baker, K., Paterson, D.M., 1999. Measuring the in situ erosion shear stress of intertidal sediments with the cohesive strength meter (CSM). Estuarine Coastal and Shelf Science 49, 281–294.

Tolhurst, T.J., Black, K.S., Paterson, D.M., Mitchener, H.J., Termaat, G.R., Shayler, S.A., 2000a. A comparison and measurement standardization of four in situ devices for determining the erosion shear stress of intertidal sediment. Continental Shelf Research 20, 1397–1418.

Tolhurst, T.J., Reithmuller, R., Paterson, D.M., 2000b. In situ versus laboratory analysis of sediment stability from intertidal mudflats. Continental Shelf Research 20, 1317–1334.

Traykovski, P., Wiberg, P.L., Geyer, W.R., 2007. Observations and modeling of wave-supported sediment gravity flows on the Po prodelta and comparison to prior observations from the Eel shelf. Continental Shelf Research 27, 375–399.

van Ledden, M., van Kestern, W.G.M., Winterwerp, J.C., 2004. A conceptual framework for the erosion behaviour of sand-mud mixtures. Continental Shelf Research 24, 1–11.

Wheatcroft, R.A., Sanders, R.S., Law, B.A., Seasonal variation in physical and biological factors that influence sediment porosity on a temperate mudflat: Willapa Bay, Washington, USA. Continental Shelf Research, this volume.

Wiberg, P.L., Drake, D.E., Cacchione, D.A., 1994. Sediment resuspension and bed armoring during high bottom stress events on the northern California continental shelf: measurements and predictions. Continental Shelf Research 14, 1191–1219.

Wiberg, P.L., Sherwood, C.R., 2008. Calculating wave-generated bottom orbital velocities from surface-wave parameters. Computers & Geosciences 34, 1243–1262.

Widdows, J., Brinsley, M.D., Bowley, N., Barret, C., 1998. A benthic annular flume for in situ measurements of suspension feeding/biodeposition rates and erosion potential of intertidal cohesive sediments. Estuarine Coastal and Shelf Science 46, 27–38.

Widdows, J., Brown, S., Brinsley, M.D., Salkeld, P.N., Elliott, M., 2000. Temporal changes in intertidal sediment erodibility: influence of biological and climatic factors. Continental Shelf Research 20, 1275–1289.

Widdows, J., Friend, P.L., Bale, A.J., Brinsley, M.D., Pope, N.D., Thompson, C.E.L., 2007. Inter-comparison between five devices for determining erodibility of intertidal sediments. Continental Shelf Research 27, 1174–1189.

Wunsch, C., Stammer, D., 1997. Atmospheric loading and the oceanic "inverted barometer" effect. Reviews of Geophysics 35, 79–107.